Supplementary Information

Synergetic effects of cation and anion of $Mg(NO_3)_2$ as electrolyte additives in stabilizing Li metal anode

Hyerim Kim[a,†], Jimin Park[a,†], Hyokyeong Kang[a], Sunggun Lim[b], Shivam Kansara[a], Zhaowei Sun[c,*], Shizhao Xiong[c,*], Yun-chae Jung[d], Chihyun Hwang[d], Marco Agostini[e], and Jang-Yeon Hwang[a,b,*]

[a]*Department of Energy Engineering, Hanyang University, Seoul 04763, Republic of Korea*
[b]*Department of Battery Engineering, Hanyang University, Seoul 04763, Republic of Korea*
[c]*Faculty of Material Science and Engineering, Kunming University of Science and Technology, Kunming, 650093, China*
[d]*Batteries Research Center, Korea Electronics Technology Institute, Seongnam, Gyeonggi 13509, Republic of Korea*
[e]*Department of Chemistry and Drug Technologies, Sapienza University of Rome, P.le Aldo Moro 5, Rome 00185, Italy*

Corresponding author: jangyeonhw@hanyang.ac.kr

[†]These authors contributed equally to this work.

Experimental Section

Treatment of raw materials

Lithium hexafluorophosphate ($LiPF_6$, Sigma–Aldrich) was dried under a vacuum at 80 ℃ in a vacuum oven (Buchi) for 80 h. The $Mg(NO_3)_2{\cdot}6H_2O$ powder ($Mg(NO_3)_2$, Sigma–Aldrich) was vacuum dried at 40 °C in the vacuum oven for 72 h. Lithium difluoro(oxalato)borate (LiDFOB, Sigma–Aldrich) was vacuum dried at 110 °C in the vacuum oven for 72 h. Ethyl methyl carbonate (EMC, TCI), fluoroethylene carbonate (FEC, TCI), and γ-butyrolactone (GBL, Daejung Chemicals) solvents were purified twice using 4 Å molecular sieves. Polyacrylonitrile (M.W. 150,000) (PAN, Sigma–Aldrich) and sulfur (trace metals basis 99.998%) (S, Sigma–Aldrich) were used to synthesize the sulfurized polyacrylonitrile (SPAN) powder.

Electrolyte preparation

To reveal the functions of $Mg(NO_3)_2$ as an additive and GBL as mediator, six electrolyte samples were prepared; 1) the baseline electrolyte, was prepared by dissolving 1 mol L^{-1}(M) $LiPF_6$ and 0.05 M LiDFOB in a solution of EMC and FEC (at a volume ratio of 3:1), 2) the **GBL-only electrolyte**, was prepared by adding 0.25 g of GBL to 2 mL of the baseline electrolyte, 3) the **$Mg(NO_3)_2$-only** electrolyte, was produced by adding only 0.1 M $Mg(NO_3)_2$ to the baseline electrolyte without GBL solvent, and 4) the **0.1 $Mg(NO_3)_2$-GBL** electrolyte, was prepared by two-step process. First, 0.93 M $Mg(NO_3)_2$ additive is added to the GBL solvent. Then, 0.24 mL of this solution is added to 2 mL of baseline electrolyte. Finally, 2.24 mL of electrolyte consisting of 0.1 M $Mg(NO_3)_2$ and 0.2554 g of GBL solvent is made. In the same manner, 5) **0.2 $Mg(NO_3)_2$-GBL** and 6) **0.3 $Mg(NO_3)_2$-GBL** electrolytes were prepared, respectively. To prepare 5) **0.2 $Mg(NO_3)_2$-GBL** electrolyte, 1.86 M $Mg(NO_3)_2$ additive is added to the GBL solvent. Then, 0.24 mL is added to 2 mL of baseline electrolyte. 2.24 mL of electrolyte consisting of 0.2 M $Mg(NO_3)_2$ and 0.2383 g of GBL solvent is made. To prepare 6) **0.3 $Mg(NO_3)_2$-GBL** electrolyte, 2.8 M $Mg(NO_3)_2$ additive is added to the GBL solvent. Then, 0.24 mL is added to 2 mL of baseline electrolyte. 2.24 mL of electrolyte consisting of 0.3 M $Mg(NO_3)_2$ and 0.2222 g of GBL solvent is made.

Electrode preparation for electrochemical measurements

Li foil (99.9%, 200 μm) (Sigma–Aldrich) and Cu foil were cut into disks with diameters of 14 and 16 mm, respectively. All treatments were performed in a glovebox (H_2O < 0.1 ppm, O_2 < 0.1ppm) (MB-Unilab Max, Mbraun) under an Ar atmosphere.

The cathode for the full cell was prepared by casting a mixed slurry consisting of the active material, conductive carbon (KS6: Super P = 1:1 w/w), and polyacrylic acid (PAA) binder at a weight ratio of 8:1:1 on a carbon-coated Al foil. The active material applied in this work was SPAN, synthesized at 350 °C for 6 h in an Ar atmosphere.[S1] The average cathode active material loading level was about 2.5–3.0 mg cm^{-2}, corresponding to about 4.3–4.5 mAh cm^{-2} (1 C = 1,675 mA g^{-1}).

Fabrication of cell samples.

In this work, all cells were prepared in an Ar-filled glove box. Li/Cu asymmetric cells were fabricated using a pure Cu disk (16 mm in diameter) as the working electrode, Li metal foil (14 mm in diameter) as the reference/counter electrode, and a Celgard 2400 film as the separator in a CR2032 coin cell. Li/Li symmetric cells were assembled with Li metal foil (14 mm in diameter) as electrodes on both sides and Celgard 2400 film as a separator in CR2032 coin cells. The full cell was assembled using Li metal foil (16 mm in diameter) as the anode and SPAN as the cathode, separated with Celgard 2400 in CR2032 coin cells. SUS/SUS symmetric cells were fabricated using a spacer (16 mm in diameter) as electrodes on both sides and Celgard 2400 film as a separator in CR2032 coin cells.

Calculations and simulations.

Computational calculations were performed using density functional theory (DFT) as implemented in the Vienna Ab initio Simulation Package (VASP).[S2,S3] The Perdew-Burke-Ernzerhof (PBE) functional was employed with projector augmented-wave (PAW)-PBE pseudopotentials to describe the electronic structures of the systems accurately.[S4,S5] A plane-wave energy cutoff of 400 eV was used to ensure sufficient basis-set accuracy. Simulations were performed using a gamma-centered *k*-point grid to account for the periodic nature of the systems. For geometric optimization, the electronic convergence criterion was set to 1E-06 and the force convergence criterion was set to −1E-02, ensuring that the structural relaxations were performed with a high level of precision. The DFT-D3 method developed by Grimme[S6] was employed to account for long-range van der Waals (vdW) interactions during adsorption. This zero-damping dispersion correction scheme effectively describes the nonbonded interactions between molecules, ensuring a more accurate representation of the adsorption processes. Theoretical calculations of the highest occupied molecular orbital (HOMO)–lowest unoccupied molecular orbital (LUMO) energy levels were performed using the Gaussian 09 package. The molecular geometry was optimized using the M06-2x/6-311+G(d,p) basis set.[S7,S8]

Characterization methods

To investigate the effects of $Mg(NO_3)_2$ and GBL additives on the electrolyte, Raman spectra were collected with a Raman microscope (LabRAM Soleil, Horiba Jobin Yvon) using 532 nm excitation laser. The solvated structures of the different electrolytes were also analyzed by nuclear magnetic resonance spectrometry (NMR) (DD2 600 MHz FT NMR, Agilent Technologies). The surface and cross-sectional morphologies of the electrodes were observed using field-emission scanning electron microscopy (FE-SEM, Helios, Thermo Scientific). The main components of the SEI were detected using high-precision X-ray photoelectron spectroscopy (XPS) (Theta Probe, Thermo Scientific) and X-ray diffraction (XRD) (D8 advance, Bruker). Detailed elemental distributions across the SEI films formed in diverse electrolytes were analyzed using time-of-flight secondary ion mass spectrometry (TOF-SIMS) (TOF.SIMS-5, Ion Tof) with a 30 keV Bi^+ primary ion gun and a 2 keV Cs^+ sputter gun. The samples were carefully washed with EMC solvent to remove any possible salt residue before all observations.

Electrochemical measurements

In this study, electrochemical tests were performed using a VMP3 potentiostat (Bio-Logic). The AC impedance test was conducted from 10 mHz to 1 MHz. Average coulombic efficiency ($C.E._{avg}$) tests were performed using the as-prepared Li/Cu coin cells to reveal the reversibility of the plated Li in the different electrolytes. The CEs were calculated using the following equation[S9]:

$$C.E._{avg} = \frac{nQ_C + Q_S}{nQ_C + Q_T}$$

The charge capacity (Q_T) of 6 mAh cm^{-2} was deposited onto Cu foil, and then 1 mAh cm^{-2} of chare capacity (Q_C) was used at a current density of 3 mA cm^{-2} during cycling. After 20 cycles (n), the final stripping capacity (Q_S) was measured for calculation of CEs values.

The cycling stability of Li in various electrolytes was evaluated via galvanostatic test at various current densities. A full-battery test was conducted to demonstrate the practical value of the 0.1 $Mg(NO_3)_2$-GBL electrolyte.

The ionic conductivities (σ) of electrolyte were performed using a VMP3 potentiostat (Bio-Logic) in the range of 10 mHz to 1 MHz. The value was calculated using the following equation[S10]:

$$\sigma = \frac{l}{RA}$$

The R is resistance measured from AC impedance, A is the area of electrode and l is the thickness of Celgard 2400 film measured by micrometer (293-334, Mitutoyo).

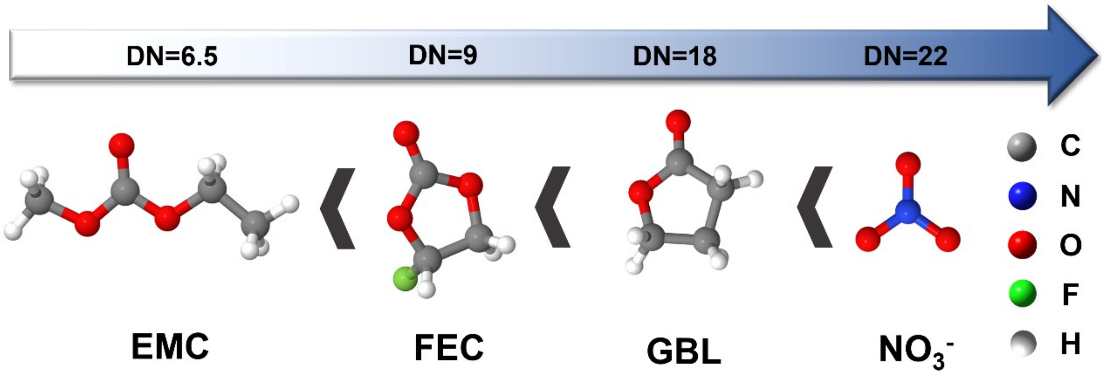

Fig. S1 A schematic comparing the Gutmann donor numbers among EMC, FEC, and GBL solvents and NO_3^- ion.

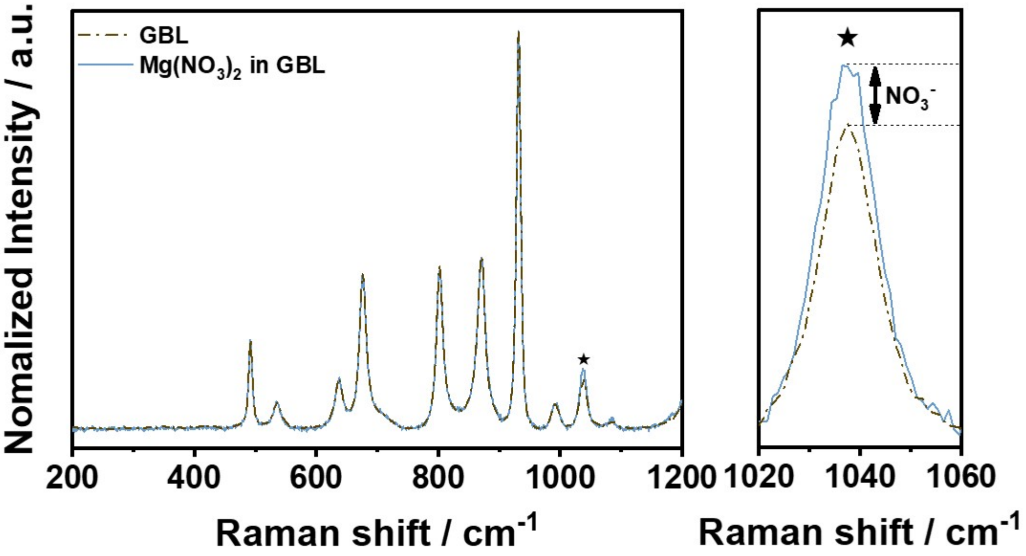

Fig. S2 Comparison of Raman spectra between the GBL solvent and $Mg(NO_3)_2$ in GBL mixture in the range of 200–1200 cm^{-1}. The enlargement shows a specific peak near 1040 cm^{-1} in the Raman spectrum that indicates the presence of NO_3^-. When comparing the spectrum of the $Mg(NO_3)_2$ in the GBL with that of the pure GBL solvent, this peak increased in intensity, indicating that the GBL solvent facilitated the dissociation of $Mg(NO_3)_2$.

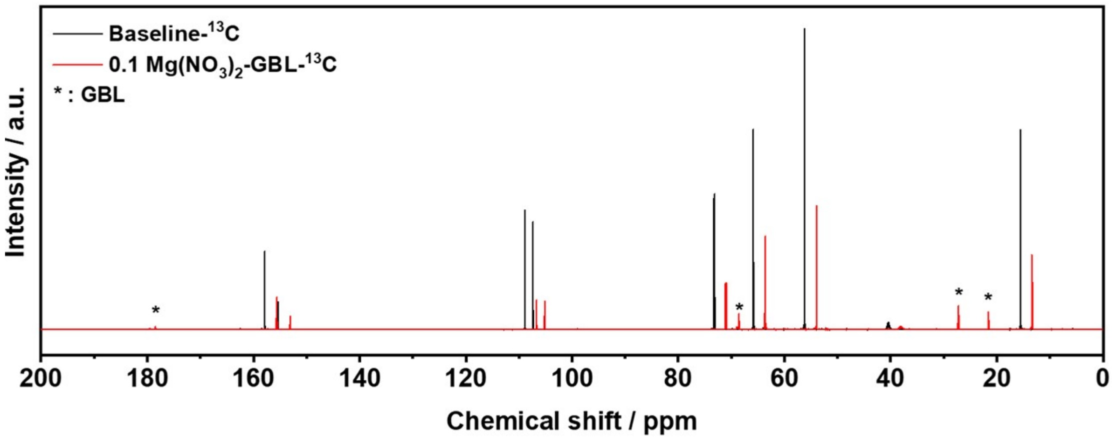

Fig. S3 Full range of ^{13}C NMR spectrum (black: baseline electrolyte, red: 0.1 $Mg(NO_3)_2$-GBL). The asterisk-marked peaks at 180, 70, 30, and 20 ppm correlate to the GBL peaks in the 0.1 $Mg(NO_3)_2$-GBL electrolyte. Chemical shifts were identified across all peaks, suggesting a change in the coordination environment.

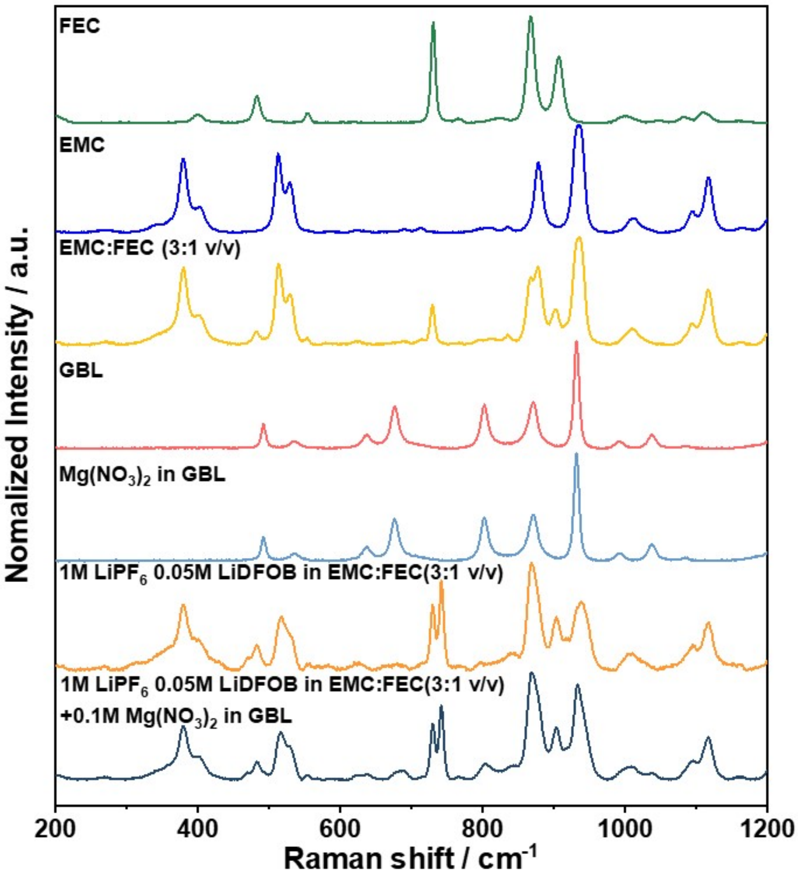

Fig. S4 The Raman spectra of FEC, EMC, EMC:FEC (3:1, v/v), and GBL solvents, as well as the $Mg(NO_3)_2$-GBL electrolyte, baseline electrolyte, and 0.1 $Mg(NO_3)_2$-GBL electrolyte. The curve of the 0.1 $Mg(NO_3)_2$-GBL electrolyte includes obvious characteristic peaks of all the other components, indicating that all the components co-exist in the 0.1 $Mg(NO_3)_2$-GBL electrolyte.

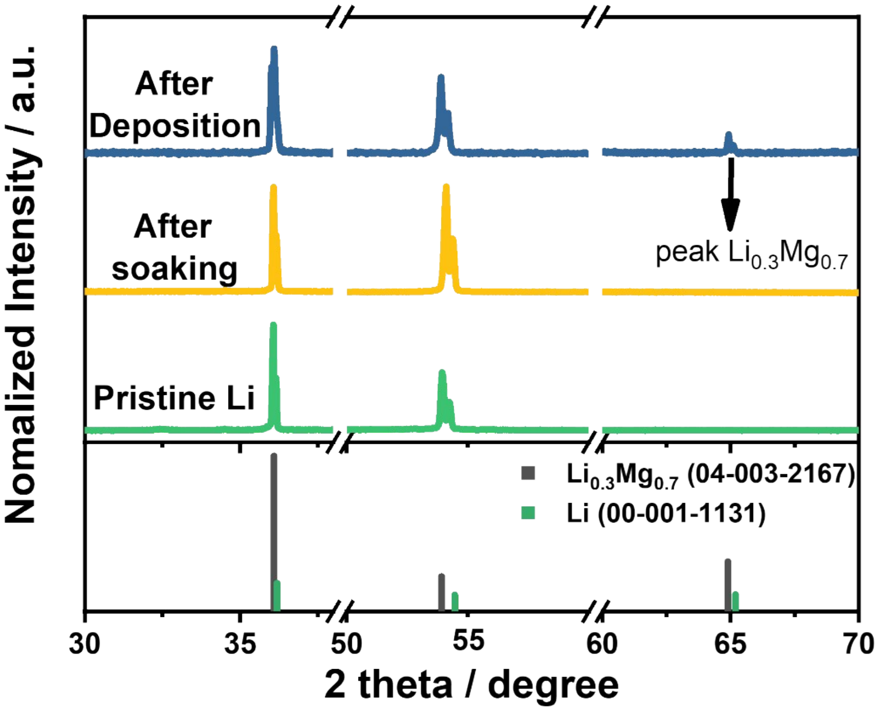

Fig. S5 XRD patterns from each state (green: pristine Li metal anode, yellow: Li metal anode after soaking for 2 h in 0.1 $Mg(NO_3)_2$-GBL, and blue: Li metal anode after deposition at a capacity loading of 4 mAh cm^{-2} and current density of 0.4 mA cm^{-2}) and reference XRD patterns from Li and $Li_{0.3}Mg_{0.7}$. The peak at 65° was not observed until after the deposition process. We suggest that this peak is attributed to the formation of Li–Mg alloy phase after the electrochemical reaction.

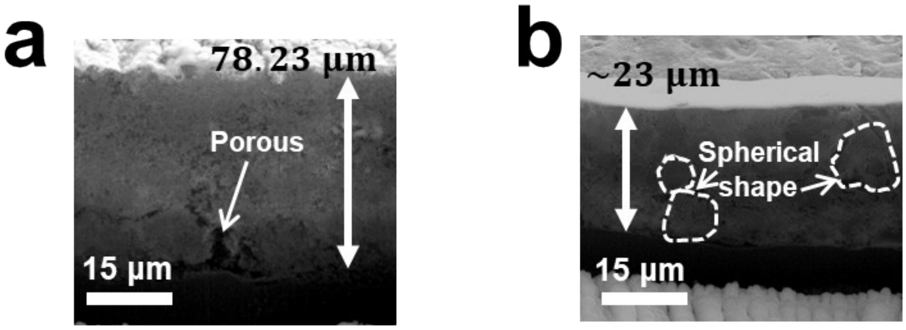

Fig. S6 Cross-sectional SEM images of (a) baseline and (b) 0.1 $Mg(NO_3)_2$-GBL electrolytes at a capacity loading of 4 mAh cm^{-2} and current density of 4 mA cm^{-2}. The baseline electrolyte has a porous surface on Li metal anode and thick and irregular deposited Li (78.23 μm). In contrast, the 0.1 $Mg(NO_3)_2$-GBL electrolyte has a dense deposited layer consisting of spherical particles (approximately 23 μm in thickness).

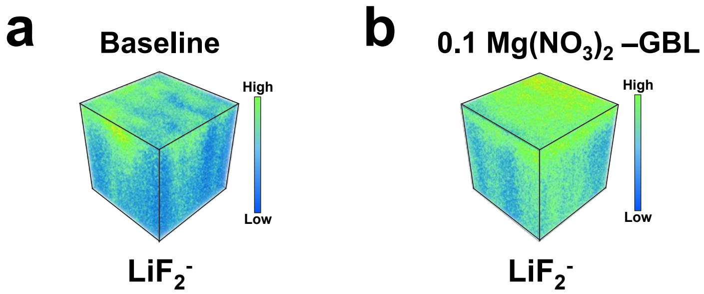

Fig. S7 3D renderings of TOF-SIMS results for the SEI layers with ion fragments of LiF_2^- using (a) baseline electrolyte and (b) 0.1 $Mg(NO_3)_2$-GBL electrolyte. This ion fragment represents LiF, and indicates that the 0.1 $Mg(NO_3)_2$ electrolyte forms a LiF-rich SEI on Li metal anode.

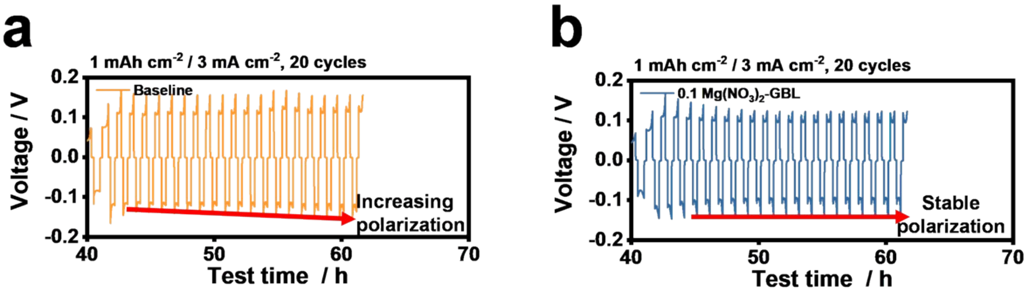

Fig. S8 Voltage profiles of Li/Li symmetric cells corresponding to the AC impedance analysis in Fig. 5b; (a) baseline and (b) 0.1 $Mg(NO_3)_2$-GBL electrolytes, respectively.

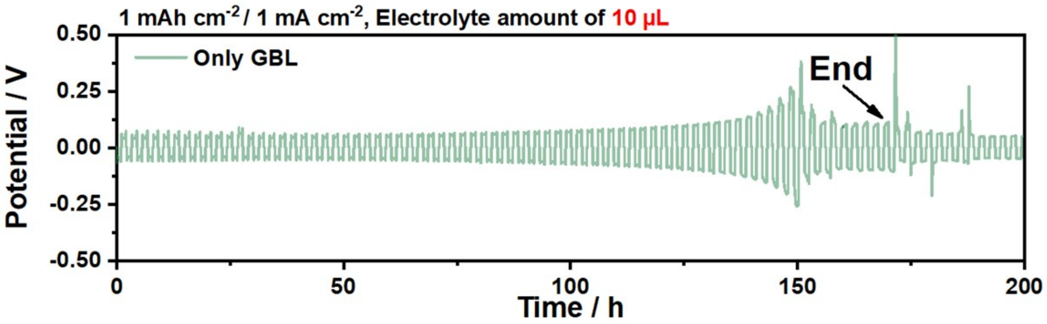

Fig. S9 Galvanostatic cycling test for Li/Li symmetric cell with only GBL added to the baseline electrolyte, proving that GBL does not affect the cycle performance. The cell used a small amount of electrolyte (10 μL) at a capacity loading of 1 mAh cm^{-2} and current density of 1 mA cm^{-2}.

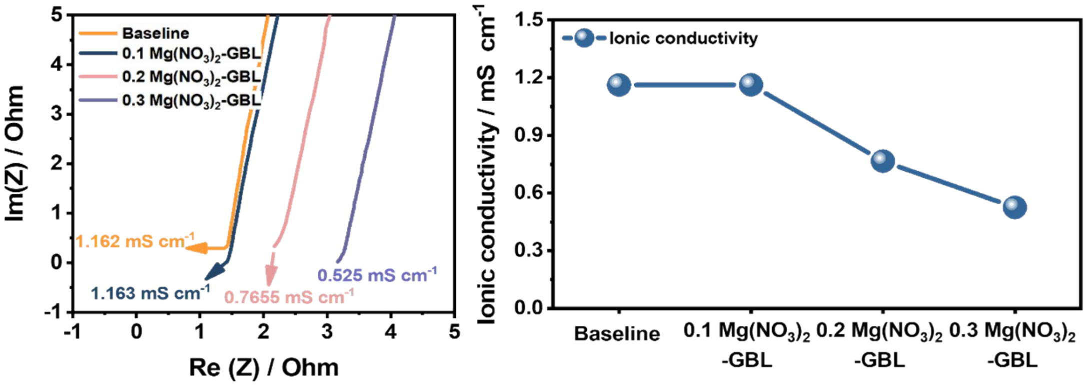

Fig. S10 Comparison of ionic conductivities corresponding to the concentration of $Mg(NO_3)_2$ additive in electrolyte using AC impedance with SUS/SUS symmetric cells in the range of 1 MHz–10 mHz. The ionic conductivities exhibited 1.163, 1.162, 0.765, and 0.525 mS cm^{-1} in baseline, 0.1 $Mg(NO_3)_2$-GBL, 0.2 $Mg(NO_3)_2$-GBL, and 0.3 $Mg(NO_3)_2$-GBL electrolytes, respectively.

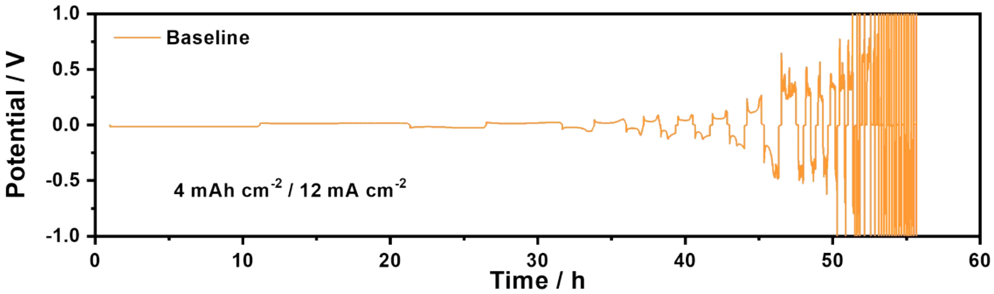

Fig. S11 Magnification of galvanostatic cycling test for Li/Li symmetric cells using the baseline electrolyte at a capacity loading of 4 mAh cm^{-2} and high current density of 12 mA cm^{-2}.

Table S1 Young's modulus and Li$^+$ conductivities of the main inorganic components in the SEI induced by Li metal anode with modified electrolyte.

Components of SEI	**LiF**	**Li-Mg alloy**	**Li_3N**	**Li_2O**	**Li**
Young's modulus (GPa)	122	~8–16	48	150	4.9
Li$^+$ conductivity (S cm^{-1})	10^{-6}	10^{-7}	10^{-3}	10^{-9}	10^{-10}

Table S2. DFT calculations of binding energies of Li^+ and Mg^{2+} to anions of NO_3^-, PF_6^-, and $DFOB^-$

Li^+	**Binding energy (eV atom^{-1})**	**Mg^{2+}**	**Binding energy (eV atom^{-1})**
NO_3^-	−1.083	NO_3^-	−0.636
PF_6^-	−0.982	PF_6^-	−0.664
$DFOB^-$	−0.616	$DFOB^-$	−0.367

References for supporting information

S1. H. Jang–Yeon, K. Hee Min and S. Yang–Kook, *J. Mater. Chem. A*, 2017, **6**, 14587–14593.

S2. G. Kresse and J. Furthmüller, *Phys. Rev. B*, 1996, **54**, 11169.

S3. G. Kresse and J. Hafner, *Phys. Rev. B*, 1993, **47**, 558–561.

S4. G. Kresse and D. Joubert, *Phys. Rev. B*, 1999, **59**, 1758–1775.

S5. J. P. Perdew, K. Burke and M. Ernzerhof, *Phys. Rev. Lett.*, 1996, **77**, 3865–3868.

S6. G. Stefan, A. Jens, E. Sterpahn and K. Helge, *J. Chem. Phys.*, 2010, **132**, 154104.

S7. D. E. Woon, T. H. Dunning and Jr., *J. Chem. Phys.*, 1995, **103**, 4572–4585.

S8. X. Lidan and B. Oleg, *Phys. Chem. Chem. Phys.*, 2012, **14**, 12838–12843.

S9. A. Brian D., Z. Jianming, R. Xiaodi, X. Wu and Z. Ji–Guang, *Adv. Energy Mater.*, 2018, **8**, 1702097.

S10. H. Zhendong, W. Yue, Z. Qing, T. Jiadong, Z. Qianqian, K. Xiaoxing, L. Jingbing, J. Yuhong and W. Hao, *Adv. Funct. Mater.*, 2021, **31**, 2102938.